sustainability

MDPI

Article

Numerical Assessment of an Air Cleaner Device under Different Working Conditions in an Indoor Environment

Farshad Moradi Kashkooli [1,†], Mostafa Sefidgar [2,†], Madjid Soltani [1,3,4,5,*], Shahab Anbari [2], Seyed-Amir Shahandashti [2] and Bahram Zargar [6]

[1] Department of Mechanical Engineering, K.N. Toosi University of Technology, Tehran 19967-15433, Iran; farshad.moradi@email.kntu.ac.ir
[2] Department of Mechanical Engineering, Pardis Branch, Islamic Azad University, Pardis 14689-95513, Iran; msefidgar@pardisiau.ac.ir (M.S.); shahab.anbari@pardisiau.ac.ir (S.A.); amir_shahandashti@pardisiau.ac.ir (S.-A.S.)
[3] Department of Electrical and Computer Engineering, University of Waterloo, Waterloo, ON N2L 3G1, Canada
[4] Waterloo Institute for Sustainable Energy (WISE), University of Waterloo, Waterloo, ON N2L 3G1, Canada
[5] Advanced Energy Initiative Center, K.N. Toosi University of Technology, Tehran 14176-14411, Iran
[6] CREM Co Labs, Mississauga, ON L4V 1T4, Canada; bzargar@cremco.ca
* Correspondence: msoltani@uwaterloo.ca
† Equal contribution.

Abstract: Transmission and spread of exhaled contaminants in the air may cause many airborne infectious diseases. In addition to appropriate ventilation, air cleaner devices are used as one of the most common ways to improve the indoor air quality. Therefore, it is necessary to understand the performance of an air cleaner under different operating conditions. This study mainly concerns investigating the effect of presence or absence of furniture and its displacement on the removal rate of the particles leaving a person's mouth while coughing in an isolated room. Moreover, the effect of air exit angle of the device on removal rate of contaminated particles and the pattern of their dispersion within a room was studied. To this aim, computational fluid dynamics were employed to examine the mentioned effects by using the Eulerian− Lagrangian method. As the results indicated, when the furniture was placed farther away from the device, more particles were removed by the device. Additionally, the air ejection angle of the air cleaner device significantly affects the removal of particles. Results of the present study could improve use of air cleaner devices for maximum reduction of particles in the indoor environment.

Keywords: air cleaner device; indoor environment; computational fluid dynamics (CFD); clean air delivery rate (CADR); particle transport

check for updates

Citation: Moradi Kashkooli, F.; Sefidgar, M.; Soltani, M.; Anbari, S.; Shahandashti, S.-A.; Zargar, B. Numerical Assessment of an Air Cleaner Device under Different Working Conditions in an Indoor Environment. *Sustainability* **2021**, *13*, 369. https://doi.org/10.3390/su13010369

Received: 13 November 2020
Accepted: 30 December 2020
Published: 3 January 2021

Publisher's Note: MDPI stays neutral with regard to jurisdictional claims in published maps and institutional affiliations.

Copyright: © 2021 by the authors. Licensee MDPI, Basel, Switzerland. This article is an open access article distributed under the terms and conditions of the Creative Commons Attribution (CC BY) license (https://creativecommons.org/licenses/by/4.0/).

1. Introduction

The negative effects of any pollutants transmitted into the indoor air may be reduced by eliminating the indoor sources of pollutants such as formaldehyde, carbon monoxide, or nitrogen oxides [1], increasing the ventilation rate [2–4], or putting air decontamination device in a given space [5–11]. In the last case, there are a series of widespread devices that claim to disinfect the indoor air based on a wide range of different technologies [12–18]. Although surveys have demonstrated that 33% of households use air decontamination devices [2], evaluation of these devices' efficacy against airborne microbial pathogens continues to be a challenge in the absence of appropriate laboratory facilities as well as credible experimental protocols. Based on Nazaroff's review article [19], indoor particle transport is affected by many factors such as the particle category, clean air delivery rate (CADR), room geometry, room surfaces roughness, and the thermal plume created through human bodies or other devices. On the other hand, the airflow pattern, the location of particle injection, and the presence of objects and obstacles against the flow can affect particle concentration at different points. In the case of coughing, the contaminative

particles have a non-uniform distribution. Relatively fewer studies reported the transport properties of the non-uniformly distributed particles in indoor environments with an air cleaner.

The three major factors which might affect the performance of air cleaner devices are the space total volume, CADR (a measure of the rate a device can clean the air by diluting the pollutants in it [20]), and the size and concentration of airborne particles [17]. To investigate the influence of different parameters on air cleaners, there exist many new efforts on mechanism [21], cleaning effectiveness description [14], CADR calculation [12,22], effects on indoor air conditions [15,16], and performance of air cleaners themselves [12,13] in the literature. In order to reduce the risk of airborne pathogens, Sattar et al. [23] studied the decontamination of indoor air using different efficacy test devices. Miller et al. [22], Kang et al. [5], Akbari and Salmanzadeh [24], and Novoselac and Siegel [6] concluded the main differences in the air decontamination level in indoor environment depending on the position of the air cleaner device.

In order to investigate the particles dispersion in an indoor environment, two major approaches including physical modeling and Computational Fluid Dynamics (CFD) simulation are used. Numerical simulation depends upon constraints and assumptions such as a controlled chamber without consideration of HVAC and room airflow. In room testing, disregard for HVAC ventilation flows can yield inaccurate results and in situ testing is more cost effective than numerical modeling. Hence, CFD is gradually being used to predict the patterns of airflow in various types of healthcare settings because of easy availability and higher sophistication [23]. Zargar et al. [25] employed CFD to find a suitable fan and its position within a chamber for uniform pathogen distribution injected into the air and to determine the room furnishing impact on airflow patterns. To evaluate and compare the effectiveness of air decontamination devices in removing the submicron-sized particles, Noh et al. [8] employed CFD for two different chambers. They also examined the CADRs and operating cost effectiveness for room air cleaner and ventilation system in a small lecture room using both experiment and numerical simulations [9]. Chen et al. [11] used CFD to investigate the efficacy of air cleaner in eliminating contaminations emitted by cigarette smoke and coughing. They concluded that the location and direction of the device play a significant role in particle concentration at different points in the room. In the work of Faulkner et al. [4], the effects of parameters such as circulation rate, particle diameter, and the location of injection of particles on particle mass concentration were examined at a few different points. Moradi Kashkooli et al. [7] developed a CFD model to evaluate the effect of the location of a commercial air cleaner device on its capacity for microbial decontamination of indoor air.

Following the literature review, in the indoor environment, air cleaner positioning requires further investigation, as it leads to different removal efficacies. In addition, the impact of air cleaner flow rate on the concentration of particles in the indoor environment is of great importance and should be taken into account. Moreover, the air exit angle to the ejection orientation of the outlet air from air cleaner device is an important factor that has not been sufficiently studied in the literature. To the best of the author's knowledge, these aspects have so far been insufficiently studied, and it is very important to understand the performance of air cleaners in different operating conditions, as the necessity of this issue has been emphasized in the literature [7,10,11,23,25]. In the present study, different boundary conditions (escape and trap) have been applied for the particle phase, while most of the previous studies only considered reflect boundary condition with uniform dispersion for particle phase. Then, a verified CFD model was used to study the effect of four factors including presence of a chair inside the room, displacement of the chair, location of the air cleaner device, as well as the angle of exit air relative to an air cleaner on dispersion and removal of the particles. The particles may be contaminations created outdoors or through respiratory tracts of the patients.

2. Mathematical Modeling

Based on the fact that the volume fraction of the particles is lower than 3%, a two-phase flow using the Eulerian−Lagrangian approach may be employed for analyzing the flow. In this approach, the flow is divided into continuous and discrete phases, where the continuous phase is the air, and the discrete phase is the polluted particles exhaled by the patient. The momentum and mass equations are examined distinctively for each phase, and the effect of the two phases on each other in every mentioned equation would be stated as the source term. In other words, the fluid phase is treated as a continuum material by solving the time-averaged Navier−Stokes equations, and the dispersed phase is solved by tracking a large number of particles through the calculated flow field.

2.1. Governing Equations of the Continuous Phase

In Eulerian−Lagrangian approach, a source term is added to the governing equations of the fluid flow. This results from the transfer of mass and momentum with the particles. Such equations may be stated as the following:

Continuity equation is in fact the law of mass conservation, and is generally written as [25,26]:

$$\frac{\partial \rho}{\partial t} + \nabla \cdot (\rho \vec{u}) = S_m \tag{1}$$

where S_m is the source term and, since there is no phase change here, this term equals zero in the equations.

Momentum equation, which is taken from Newton's second law, is as follows [25,26]:

$$\frac{D(\rho \vec{u})}{Dt} = -\nabla p + \nabla \cdot \bar{\bar{\tau}} + \rho \vec{g} + \vec{F_V} + S_p \tag{2}$$

where $\vec{u}$ and p, respectively, denote velocity vector and pressure scalar, $\bar{\bar{\tau}}$ shear stress, $\vec{g}$ gravitational acceleration vector, ρ fluid density, S_P the force applied on the fluid by particle in the unit of volume, and $\vec{F_V}$ volume forces applied to the fluid. Shear stress may be calculated as follows [26]:

$$\bar{\bar{\tau}} = \mu \left\{ \left(\nabla \cdot \vec{u} + \nabla \cdot \vec{u}_T \right) - \frac{2}{3} \left(\nabla \cdot \vec{u} I \right) \right\} \tag{3}$$

where μ and I are dynamic viscosity and unit tensor, respectively. For incompressible flows, the second term on the right equals zero.

For turbulence modeling, Reynolds-Averaged Navier−Stokes (RANS) models are used. In the present study, k-ε model will be used as the turbulence model, where k denotes the turbulence kinetic energy and ε is the rate of dissipation of turbulence energy. More information about turbulence modeling and the governing equations of the continuous phase are given in previously published works [25,27,28].

2.2. Governing Equations of the Discrete Phase

A fundamental assumption for the governing equations of the particle phase is considered here. The number of particles is so small that the volume of the particle phase is negligible compared to that of the continuous phase. Then, Eulerian-Lagrangian equations could be employed in the analysis of the problem so that the particle phase may be stated through Lagrange viewpoint, and the fluid phase may be expressed through the Eulerian point of view. The governing equations of the particle phase may be divided into the following sections:

The discrete phase trajectory is determined by integrating the force balance on the particle, which equates the particle inertia with forces acting on the particle, and can be written as the following [11,25,26]:

$$\frac{d\vec{x_p}}{dt} = \vec{u_p} \tag{4}$$

$$\frac{d\vec{u_p}}{dt} = \frac{18\mu}{\rho_p {d_p}^2}\frac{C_D \mathrm{Re}_d}{24}(\vec{u} - \vec{u_p}) + \frac{g(\rho_p - \rho)}{\rho_p} + \vec{F_m} \tag{5}$$

so that

$$\mathrm{Re}_d = \frac{\rho d_p \left|\vec{u} - \vec{u_p}\right|}{\mu} \tag{6}$$

$$C_D = \frac{24}{\mathrm{Re}}\left(1 + 0.173\mathrm{Re}^{0.657}\right) \tag{7}$$

where $\vec{u}$, $\vec{u_p}$, g, ρ_p, ρ, and $\vec{F_m}$ are the continuous phase velocity, the discrete phase velocity, the gravitational acceleration, the density of the particle, the density of the fluid, and other forces applied on the particle unit mass.

In indoor environment, the pressure gradient force, Basset force, and virtual mass force are far less than the drag force [29]; therefore, they were neglected in this study. On the other hand, the thermophoretic force, which is highly dependent upon distance and surface temperature, is negligible, because we have an isolated chamber with only the air device causing circulation, wheras the air stratification of a typical room can yield wildly differing results. Brownian and Saffman's lift forces were considered in the model, because their magnitudes are comparable to the drag force in some zones [29]. The details have been described in the literature [25,26].

The velocity of air, u, in Equation (5) consists of two components: the time-averaged component, u, and the fluctuating component, $u'(t)$ [25,26]:

$$u = \overline{u} + u'(t) \tag{8}$$

u component is calculated through the RANS equations with k-ε turbulence model. The $u'(t)$ is calculated with a stochastic method like the Discrete Random Walk (DRW). By applying the DRW model to compute $u'(t)$, the turbulent dispersion of the particle is correlated to the flow k [10,25,26]:

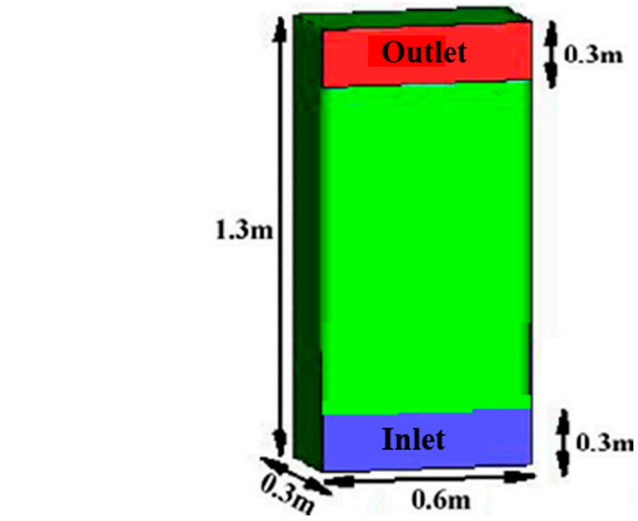
$$u'(t) = \varsigma\sqrt{\frac{2k}{3}} \tag{9}$$

in which ς is a Gaussian random number.

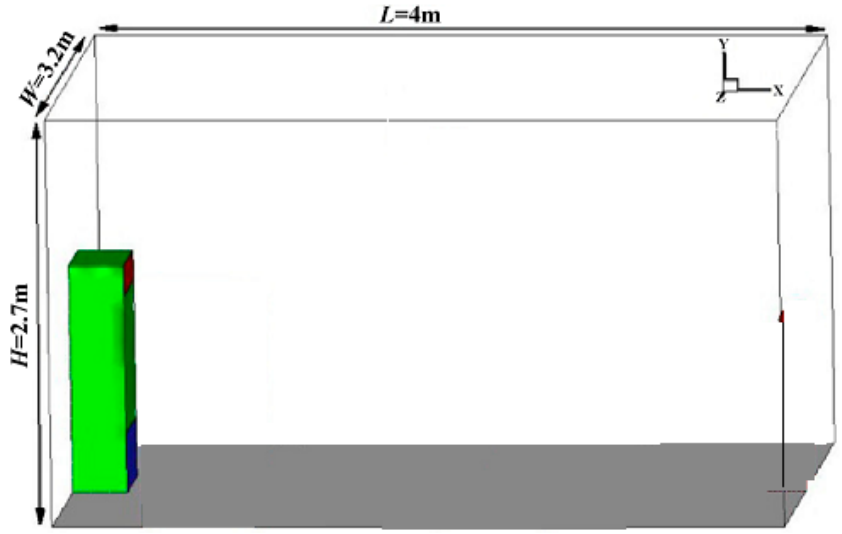
3. Material and Methods

3.1. Geometry Modeling

In this study, a room with dimensions of $4 \times 3.2 \times 2.7$ m^3 is considered. There, all of the doors and windows are closed. The airflow is created by using an air cleaner device in the room. This air cleaner has an air inlet and an outlet. The flow created through the device causes air exchange in the room. A cabinet-type air cleaner device commonly used in current households is selected from the literature [10,11]. It is assumed that the air cleaner device is placed in an isolated room without any other ventilation system. Figure 1 provides a more precise description of the problem. The axes are placed in the middle of the outlet of the air cleaner device.



(**a**) Air cleaner device



(**b**) Room and air cleaner device model

Figure 1. Geometrical modeling of the air cleaner device and room.

3.2. Definition of the Problem

A coughing source is placed exactly in front of the air cleaner device, at the other end of the room, while the device is currently in use and the airflow is under steady conditions. Suddenly, the source starts injecting the particles into the room, representing human coughs where the contaminated particles leave his mouth into the room environment. Actually, coughing was made by injecting pollutant through a hole in the wall. Therefore, geometrical shape of the human body was not modeled in this study for simplification. Due to the exchange of momentum and energy with the airflow created by the air cleaner, and under the influence of other forces (including particle weight), these particles begin to move until one of the following occurs:

- The particles collide with the walls of the chair. Here, it is assumed that the particles remain on the wall.
- The particles leave the room through the outlet of the device as shown in Figure 1a, and the device performs the removal operation through the filters placed inside the device.

The volume flow rate of the outlet air is assumed to be 600 m^3/h. Since the volume of the room is 34.56 m^3, the air exchange rate equals 17.36 ACH (Air Changes per Hour). It

is assumed that there is no ventilation (which affects the flowfield) in the room, so CO_2 may build up in the room. However, due to high ACH, complete mixing is assumed in this study.

The primary aim of this study is examining the effect of the existence of a chair (as a representative of the furniture [11]) in the room and its positioning in proportion to the device on the performance of the device in removing the particles from the room. First, in the case without a chair, the simulation is performed for two locations of the device: placing in the middle of the room width (baseline state) and in the middle of the length. Then, the chair is placed at different points in the room in order to study its effect on dispersion and removal of the particles from the room. In order to conduct this comparison, different parameters including the average pathlines of the particles, the time required for removing all the particles from the room, and the number of particles entering the air cleaner outlet will be addressed.

The secondary aim of this study is investigating the effect of outlet angles of the air on the device performance in removal of the particles from the room. Here, it is required to change the velocity angle at the inlet of the device by keeping the flow rate constant, and the distribution of the particles in the room may be obtained in each case through numerical solutions. Finally, by comparing the results, the effect of changing the angle should be investigated.

In order to simulate the coughing phenomenon, as conducted in [20], the outlet rate for the person's mouth equals 1.4 m^3/h, and the particle velocity may, therefore, be approximately estimated as 20 m/s. Additionally, the duration of the coughing process is assumed to be 0.5 s. Figure 2 indicates variations in the injected particle velocity versus time in the coughing phenomenon.

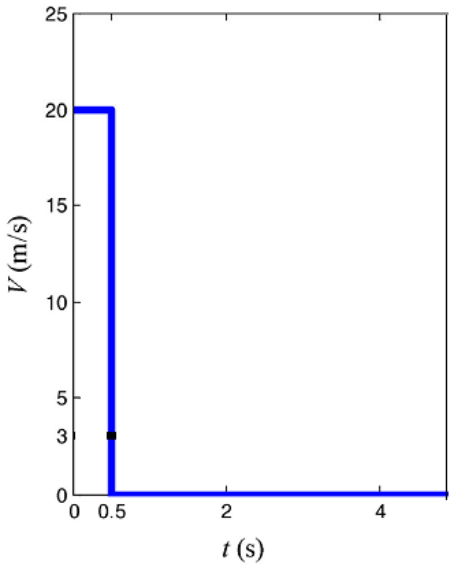


Figure 2. Variation of the injected particle velocity versus time in the coughing phenomenon.

It should be noted that, when coughing, a person normally does more than one cycle of this action; however, due to a high computational cost, the assumption is that it occurs only once. Such simplification will be enough to study the characteristics of the particle transport phenomenon in the fluid [20]. According to Miller's work [30], the diameter of the particle resulting from coughing is approximately 1µm, and the number of particles is considered 3000. Additionally, the particles density is 1200 kg/m^3.

3.3. Numerical Modeling

Grid generation descriptions, solver settings, and boundary conditions will be addressed in this section. It is noteworthy that the Ansys Fluent commercial CFD code [26] has been used in this work for processing the steps of flow solution.

3.3.1. Grid Generation

First, the computational space geometry is generated as shown in Figure 3 with the present of room, air cleaner device, and chair. Here, in order to examine the effect of the chair's position on particle removal, the location of the chair is denoted by the variable of x. Then, in order to study the displacement of the air cleaner device, the device is placed in two different positions: in the middle of the smaller side of the room, and in the middle of the larger side.

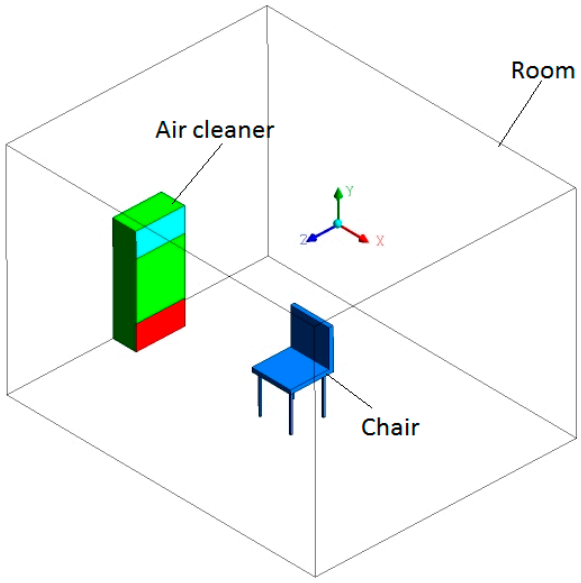
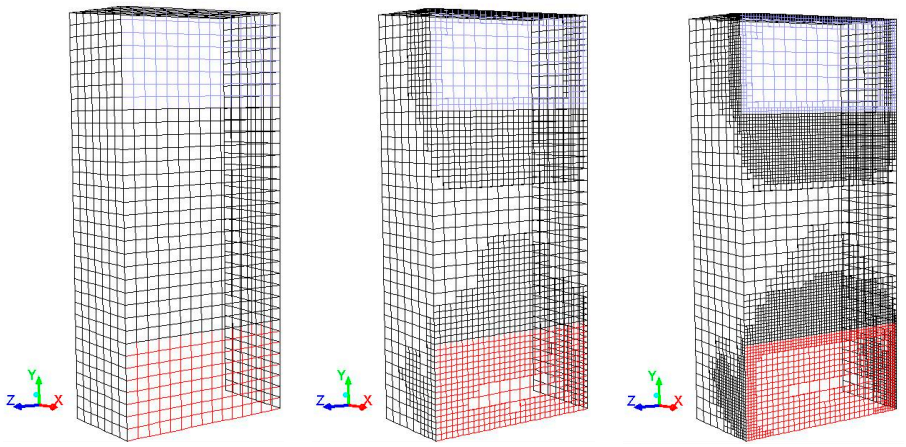


Figure 3. The physical model of the computational domain.

The physical model is composed of three parts including the air cleaner, the chair, and different geometric configurations. Grids are created for each part separately and then connected to generate the whole grid. For the primary model, the size of each cell is defined 0.04 m, and a grid with 954,132 cells is selected as an optimum mesh. It should be noted that in the following steps in the solver, adapting tools are used in order to fine the grids in the required locations. It should be mentioned that during the solving process, the grid adapt is automatically used so that such an operation is done based on velocity gradients after every 50 iterations. Hence, the grid is automatically finer in the areas where the velocity has a stronger gradient. In other words, first the simulation starts with a simple mesh, then the software solves the problem. Based on the velocity simulation results in each iteration, the software makes the mesh smaller in areas where there is a velocity gradient in the next iteration. This process continues for up to 50 iterations, reaching the ideal mesh. Figure 4 illustrates the result of the finer grid by adapting it to the velocity gradient.

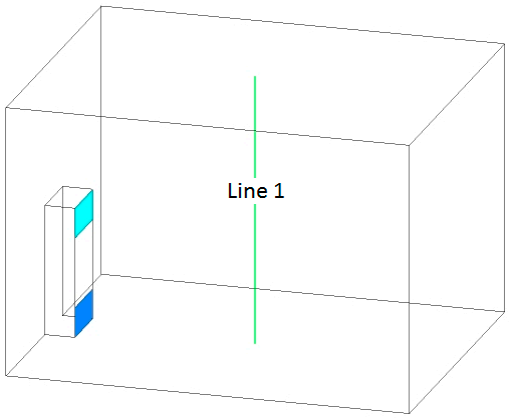
In order to ensure the results of the continuous phase solution, in the case without a chair, the independency of the results from the grid is studied as well as positioning the cleaning device in the middle of the small side. In other words, the adapting operation is continued for so long as to make the grid small enough not to change the results any further. To this aim, Line 1 is defined, and the velocity profile on this line is drawn for different grids until the profile is rationally constant by fining the grid further. The location of this line is in the middle of the computational space in the direction of y-axis, as shown in Figure 5a. The results of the solution for different grids are shown in Figure 5b in order

to examine the grid independency of the solution, which implies that a grid with 945,132 cells has reported relatively appropriate results.

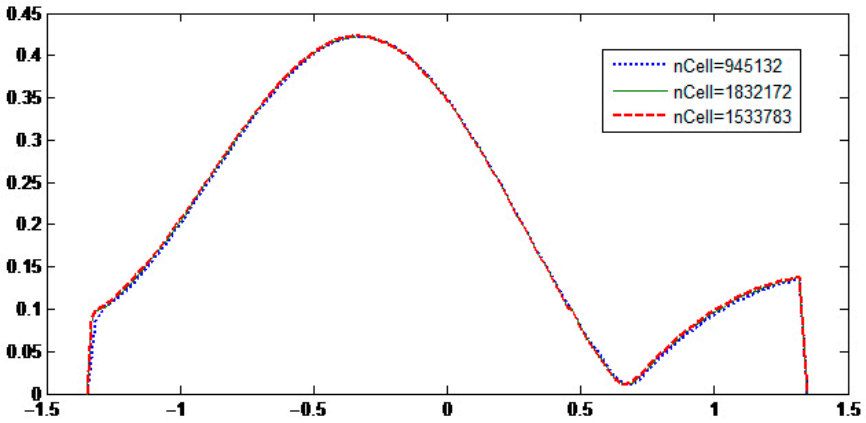


(**a**) Original grid (**b**) 1st adapt (**c**) 2nd adapt

Figure 4. Results of finer grid by adapting to velocity gradient.



(**a**) Line 1 position in computational domain

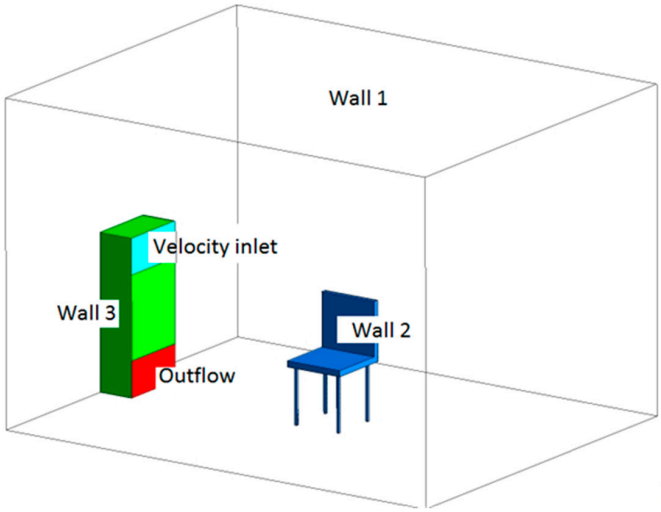


(**b**) Variations of velocity profile versus place on Line 1 for three different grids

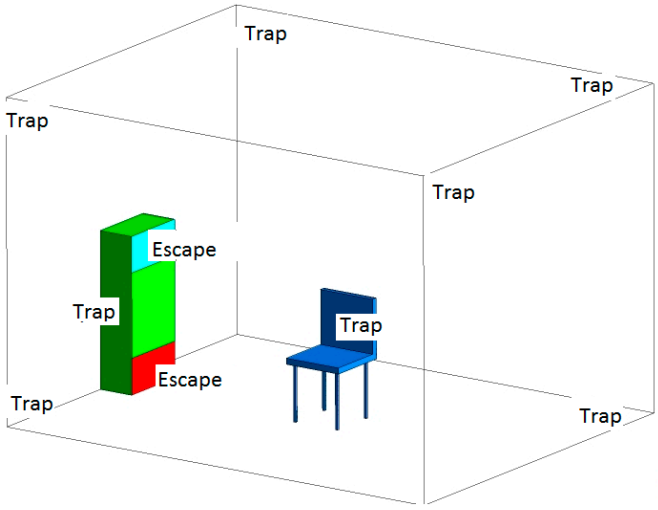
Figure 5. Grid independency test on Line 1 (**a**) Line 1 position in computational domain (**b**) Variations of velocity profile versus place on Line 1 for three different grids.

3.3.2. Boundary Conditions

Three types of boundary conditions have been applied in the present study for the continuous phase. The walls of the room, the air cleaner device, and the body of the chair are all defined as "walls". The outlet of air from the device towards the room is defined as "velocity inlet" (the velocity inlet of 0.93 m/s is applied to provide the intended flow rate), and the outlet of air from the room towards the device as "outflow". Figure 6a illustrates these boundary conditions and their location.



(**a**) Continuous phase



(**b**) Discrete phase

Figure 6. Boundary conditions for (**a**) continuous phase (**b**) discrete phase.

There are different options including escape and trap on boundary condition for the particle phase. If a particle reaches the escape boundary condition, it means that it has been removed from the computational domain, and the solver will remove it from the calculation cycle in the next time step. Here, the velocity inlet and outflow boundary conditions for the particle phase are defined as the escape, and the boundary condition of the wall type is considered as the trap. Figure 6b depicts the boundary conditions of the particles in the computational domain.

3.3.3. Solver

The three-dimensional incompressible Navier−Stokes equations were utilized to model the flow field by using finite volume method. The commercial CFD code of ANSYS

FLUENT is used as the solver for the simulation process. For the viscous and convection terms, the second-order accuracy and second-order upwind scheme were employed, respectively. The SIMPLE algorithm was used to handle the pressure−velocity coupling. For all equations, the convergence condition was satisfied with the criteria of 1×10^{-5} and in some cases with the criteria of 5×10^{-6}. As it is described in Section 2, the Eulerian−Lagrangian approach was implemented directly using the discrete phase model (DPM). In this approach, the fluid phase is treated as a continuum material by solving the time-averaged Navier−Stokes equations, and the dispersed phase is solved by tracking a large number of particles through the calculated flow field. The solution strategy primarily entails solving the flow with no consideration of the particles resulting from the cough. k-ε turbulence model is used for solving the continuous flow of the fluid. Then, the transient study is started. As mentioned, in order to study particle transport, the DPM is employed and the process of particle injection is adjusted. The parameters, related to interactions of the particles and the continuous phase, are defined here. The drag force affecting the sphere, and Suffman and Brownian forces are assumed for the calculations as the influential forces applied from both phases on each other. Additionally, the solution for particles is adjusted under unsteady conditions so that the time step is equal to 0.02 s. Particles injection is set in such a way that in every time step of the particle phase, a value of 120 particles begin to move at a rate of 20 m/s as a cone of 3 cm diameter in a 30-degree angle. Injection of these particles continues for 0.5 s, according to Figure 2, and then the injection stops.

3.4. Validation

In order to verify the results in this study, the problem addressed by Jin et al. [10] has been investigated. Instead of running five injections with a diameter of 1–5 μm, one injection is applied with a Rosin−Rammler type of dispersion with the minimum diameter of 1 μm, the maximum of 5 μm, and the average of 2.5 μm. Then, the numerical solution has been applied for 1100 s. Eventually, the average concentration of particles in a whole room versus time is calculated as shown in Figure 7. As is clear, the results of the present study are well in correspondence with the experimental results [29,31], with a higher accuracy compared to the work of Jin et al. [10]. Additionally, it is showing that the current models and methods are enough reliable to predict the particle transport in the room with an air cleaner.

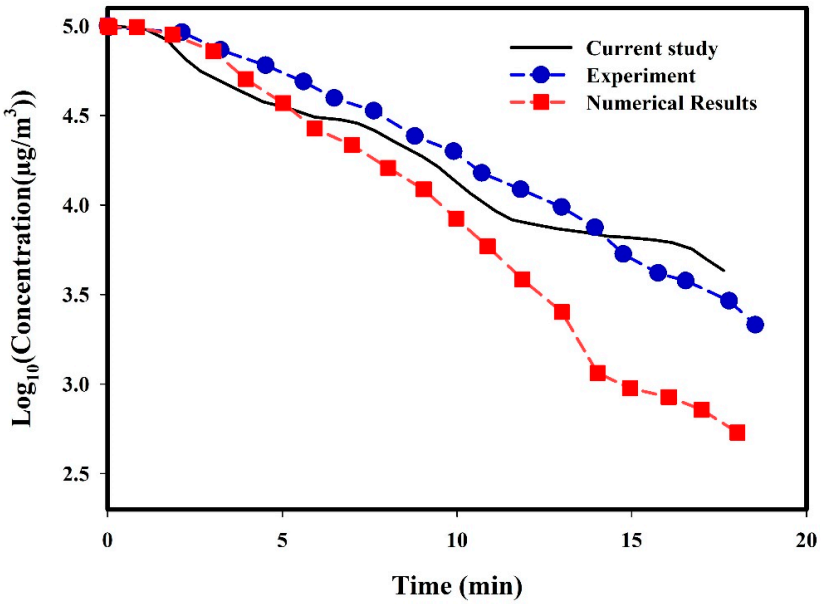


Figure 7. A comparison between the results of the current study and the numerical Jin et al. [10] and experimental (Zhao et al. [29]) results.

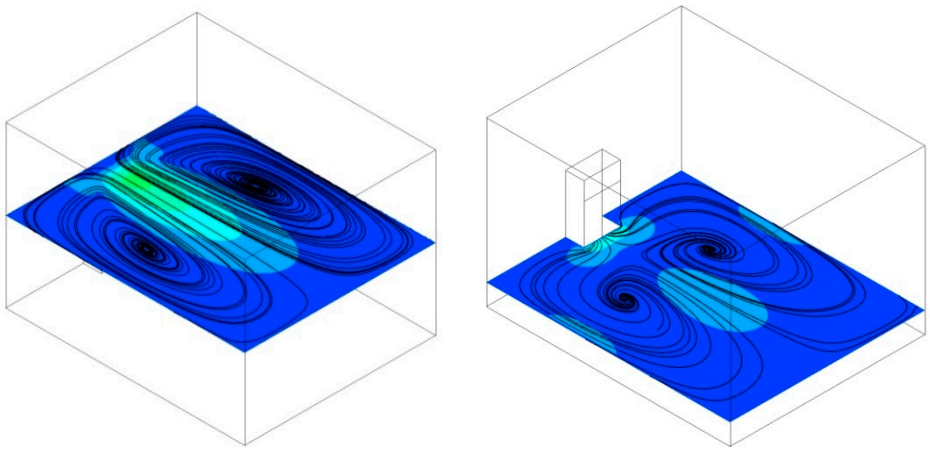
4. Results and Discussion

In the following, the results have been presented in seven distinct sections in order to examine the problem. The topics addressed will include study of the fluid flow, streamlines, and pathlines under different working conditions; study of displacement of the air cleaner device and room furniture; and study of the air exit angle to the air cleaner device (relative to *y*-axis and *z*-axis).

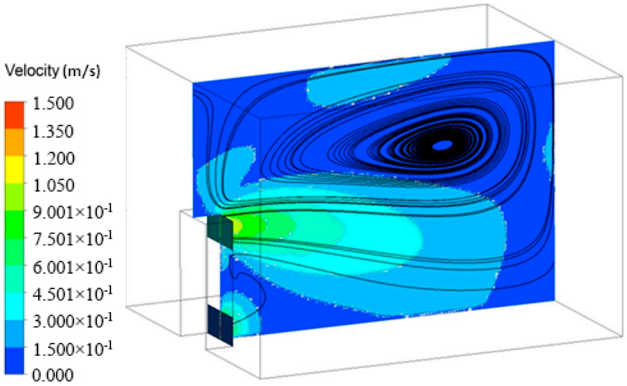
4.1. Fluid Flow, Streamlines, and Pathlines under Different Working Conditions

In this section, the problem has been examined first in the cases without the presence of a chair in two positions of the device, in the middle of length and width, in which case the chair is placed in the center of the room and device in the middle of the width. Then, the chair is relocated and moved from the center to the other end of the room, and the effect of this positioning on the pattern of particle movement has been investigated.

Initially, the normal case, i.e., placing the device on width in the absence of a chair, is addressed. For further investigation, streamlines and velocity distributions have been demonstrated in different sections of the room in Figure 8. As is obvious in Figure 8, there are vortices formed in different directions, and they cause further dispersion of the particles in transverse directions. Figure 8c demonstrates streamlines and velocity distributions on a longitudinal plane of the room. As was expected, gradients and velocity values near the inlet and outlet of the device were higher than those in other parts of the room.



(**a**) y = 0 plane (**b**) y = −1 m plane

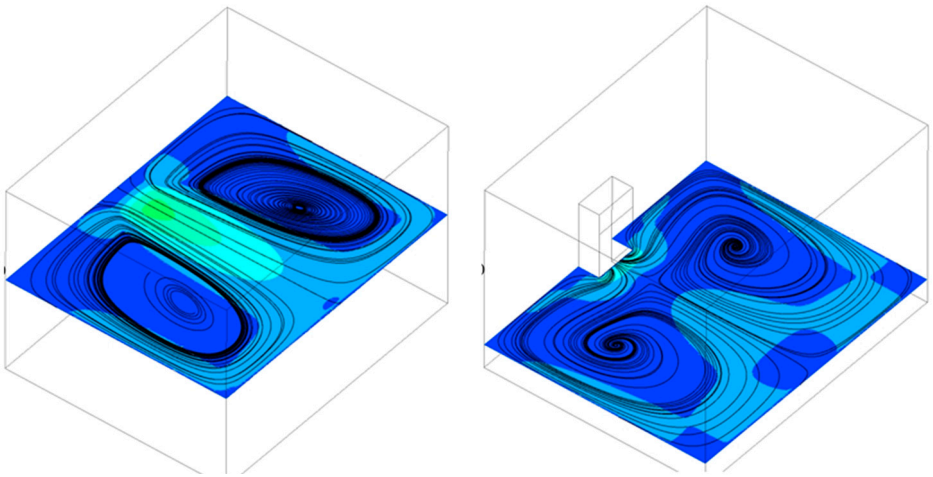


(**c**) z = 0 plane

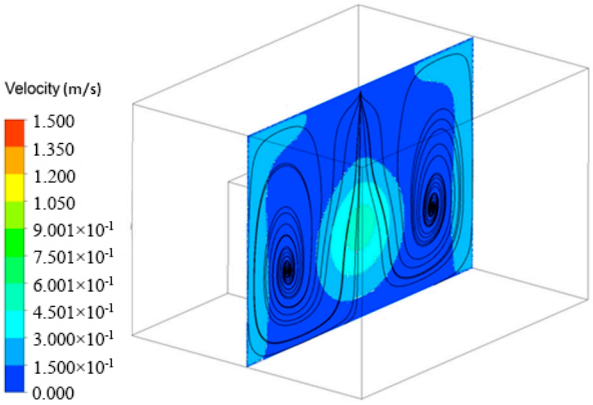
Figure 8. Streamlines and velocity distribution on different planes in the case without the presence of a chair.

In the case where the device is relocated and placed in the middle of room length, the results were obtained as presented in Figure 9. As is obvious in Figure 9c, symmetrical

vortices have been formed. These vortices are almost the same as those in the previous case with regards to symmetry, but they are different in direction and pattern. In fact, with the placement of the device in the middle of the larger side, the longitudinal vortex in the previous case is vanished and changed into two smaller vortices. In the following sections, the effect of such pattern change on particle movement will be addressed.



(**a**) y = 0 plane (**b**) y = −1 m plane

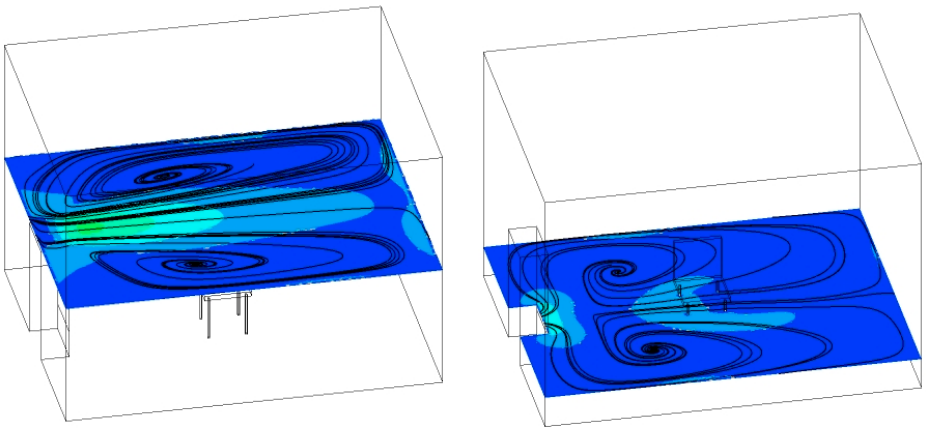


(**c**) z = 0 plane

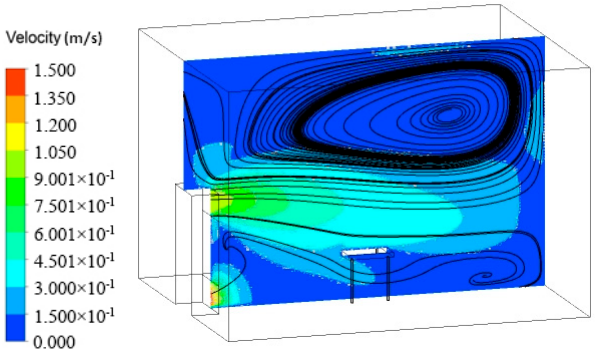
Figure 9. Streamlines and velocity distribution on different planes in the case of placing the device in the middle of the room length.

In the third step, by adding the chair to the middle of the room, the streamlines and velocity distribution for different planes are obtained as Figure 10. According to Figure 10c and by comparing it to streamlines in the case without a chair in Figure 9c, the change in streamlines in longitudinal state is evident. Consequently, another vortex has appeared at a distance from the floor up to a height approximately equal to the seating plane of the chair. If a particle enters this area, it will experience a different path from that in the case without a chair.

So far, the results of the continuous phase have been studied. In the following, the results obtained from particle injection and the pattern of particle transport will be addressed. Figure 11 illustrates the pattern of particle transport after injection in the case of placing a chair at x = 2.5 m. From the comparison of Figure 11a–e and the streamlines in Figures 8–10, it may be concluded that the particles move under the influence of the longitudinal vortex. In general, the pathlines of the particles highly complies with the trend of the streamlines of the continuous phase.

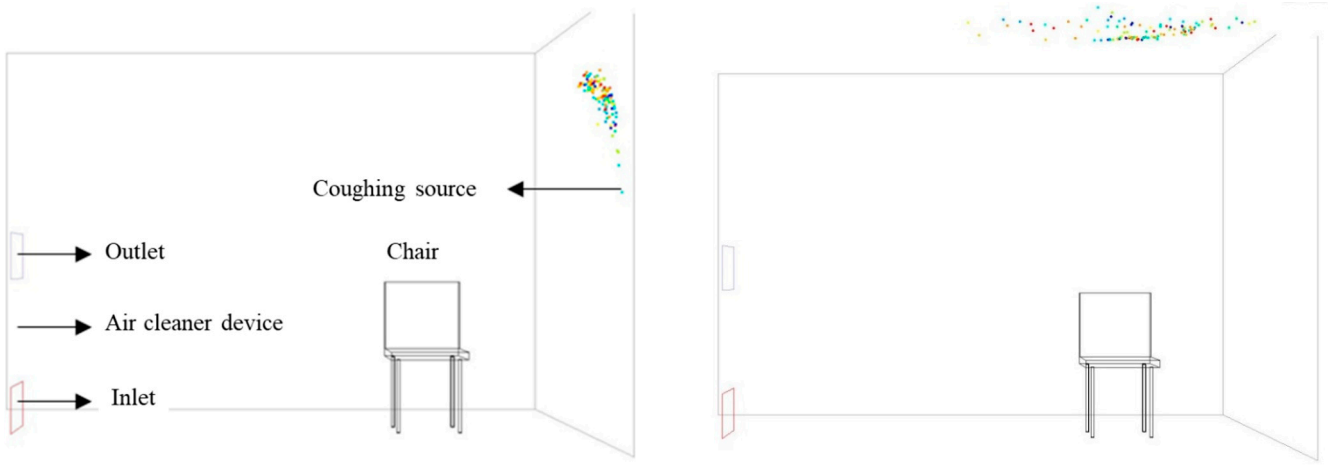


(**a**) y = 0 plane (**b**) y = −1 m plane



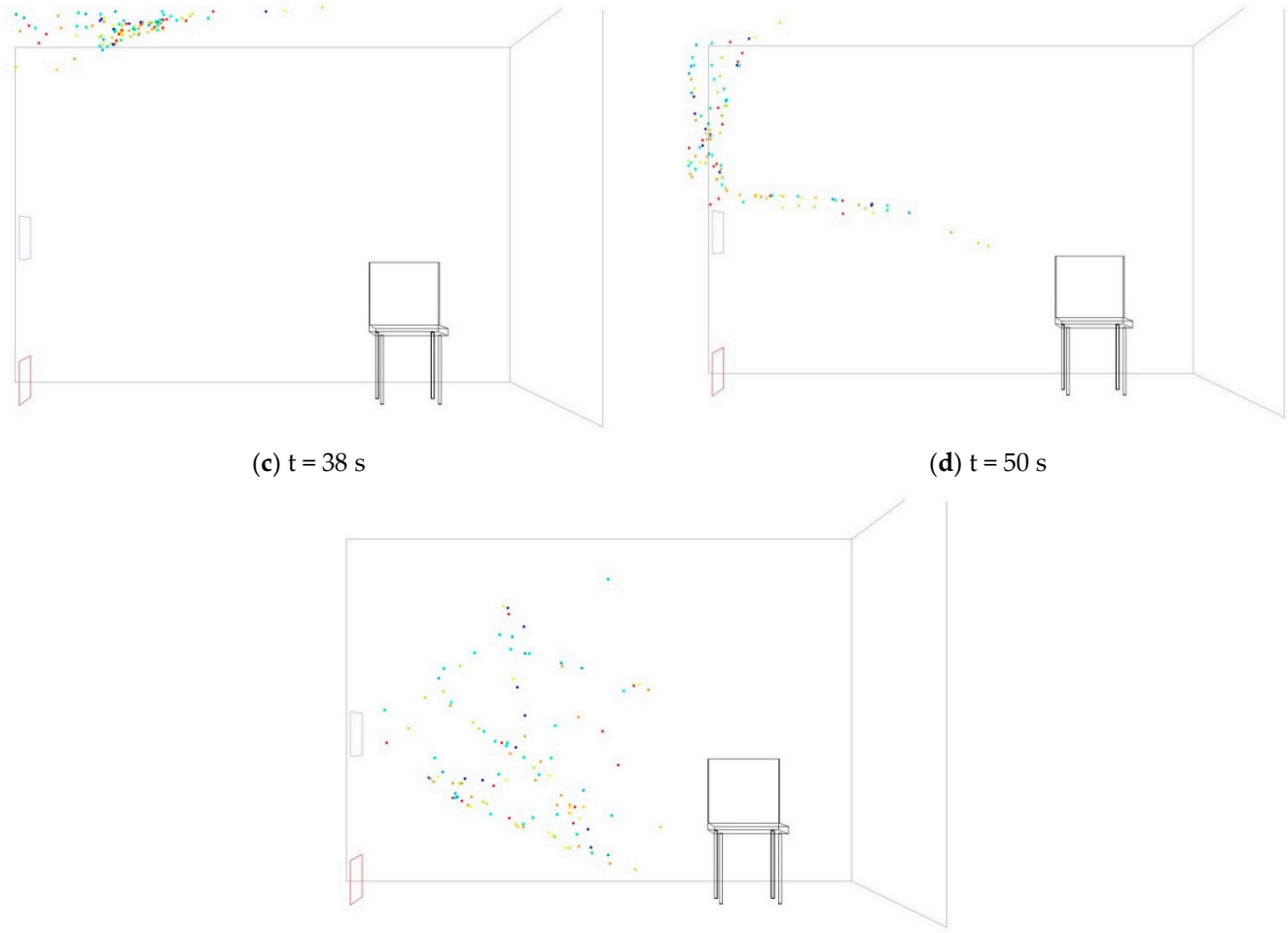
(**c**) z = 0 plane

Figure 10. Streamlines and velocity distribution on different planes in case of a chair in the center.



(**a**) t = 1 s (**b**) t = 2.5 s

Figure 11. *Cont.*

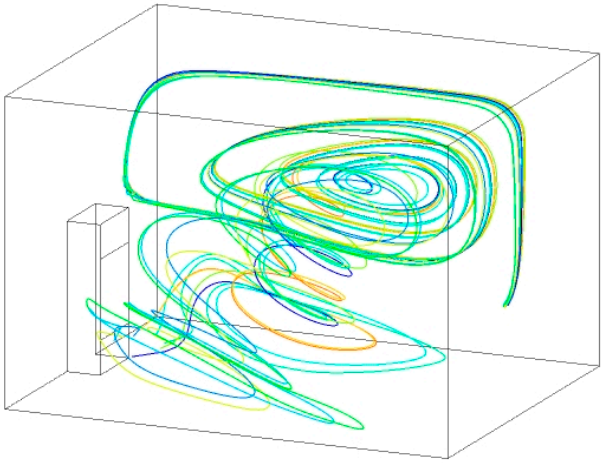


(**c**) t = 38 s (**d**) t = 50 s

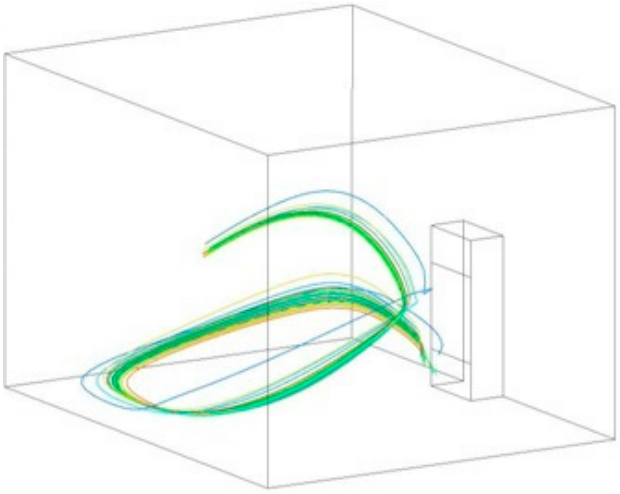
(**e**) t = 150 s

Figure 11. A view of particle position at different times post-injection (**a**) t = 1 s (**b**) t = 2.5 s (**c**) t = 38 s (**d**) t = 50 s (**e**) t = 150 s.

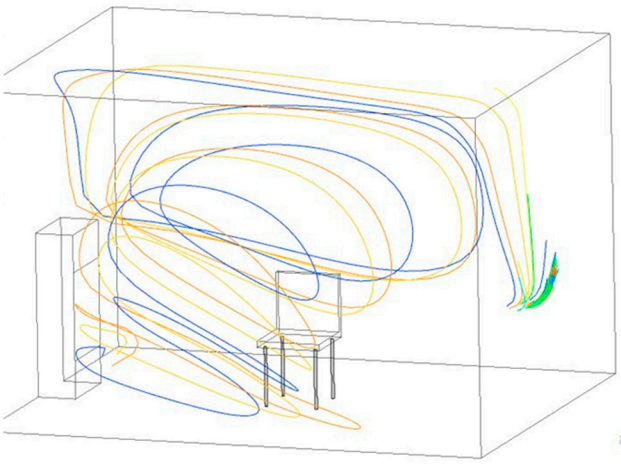
Figure 12 shows the pathlines of a number of particles selected randomly. In the case with a chair present in the room (Figure 12c), only a few of the particles reached the outlet, most of which collided with the wall at the first moments of injection. Particle dispersion is another property of this case. Figure 12a illustrates the effect of removing the chair from the room space. In this case, also, the particle movement contains irregularities, but almost all of the particles reach the device inlet. Figure 12b presents the pathlines of particles in the case of placing the device in the middle of the length. As is clear, the particles follow an approximately similar path, and almost all of them have reached the device inlet.



(**a**) Placing the device in the middle of the room width, without the chair



(**b**) Placing the device in the middle of the room length, without the chair

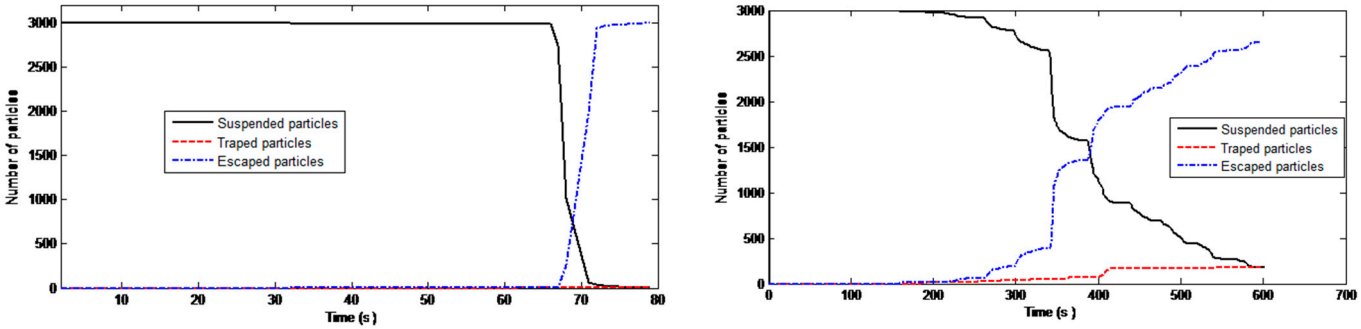


(**c**) Placing the device in the middle of the room width in the presence of the chair

Figure 12. The pathlines of a number of particles randomly selected in the room in different states.

4.2. Displacement of Air Cleaner Device

This section conducts a more accurate study of the effect of displacing the air cleaner device on the pattern of dispersion and particle removal. With an initial comparison between Figure 13a,b; it seems, when the device is in the middle of the length, all particles follow a relatively constant path and reach the outlet faster. In order to compare these states and to determine which state can guide the particles towards the device outlet faster than the other, the number of the suspended particles in room space is plotted at different moments for both of the mentioned states. A comparison of Figure 13a,b indicates the effect of the air cleaner device displacement. In the case of placing the device in the middle of the room length, the particles leave the room approximately eight times faster. Additionally, according to Figure 14, it may be seen that a much smaller number of particles will stick to room walls in the case of placing the device in the middle of the length.



(**a**) In the middle of the room length (**b**) In the middle of the room width

Figure 13. Particle situation versus time for no chair state in two different positions of device.

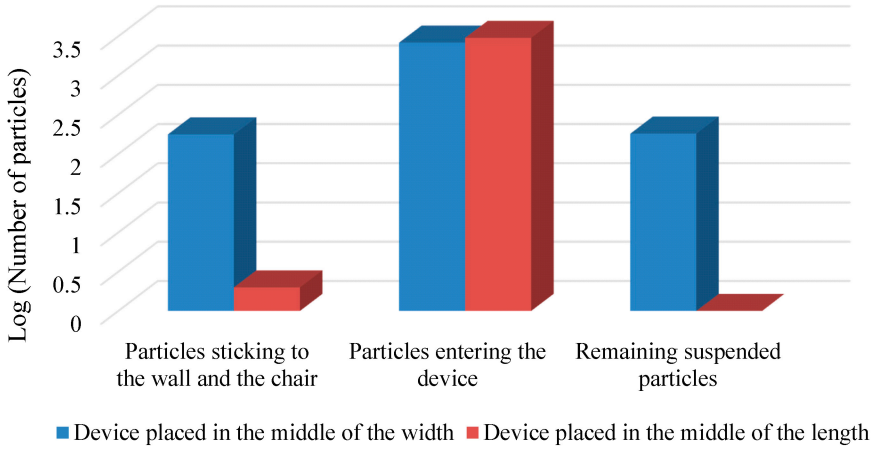
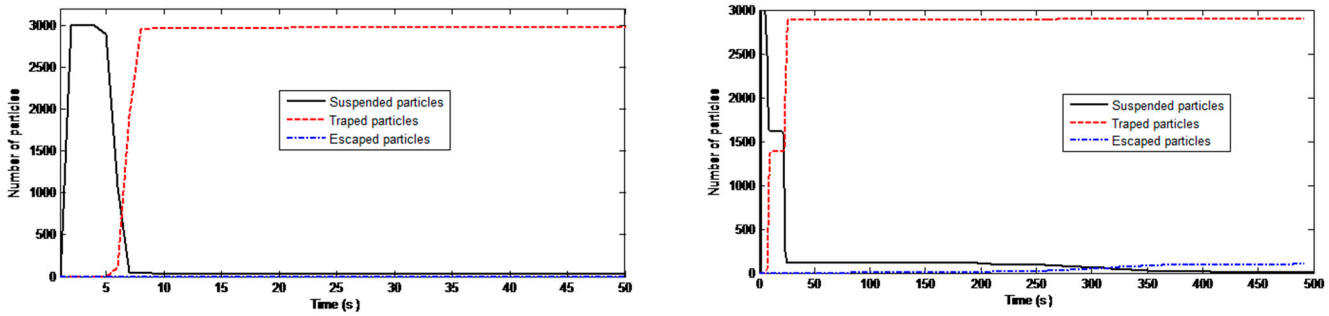


Figure 14. The final situation of the particles in the case of displacing the air cleaner device.

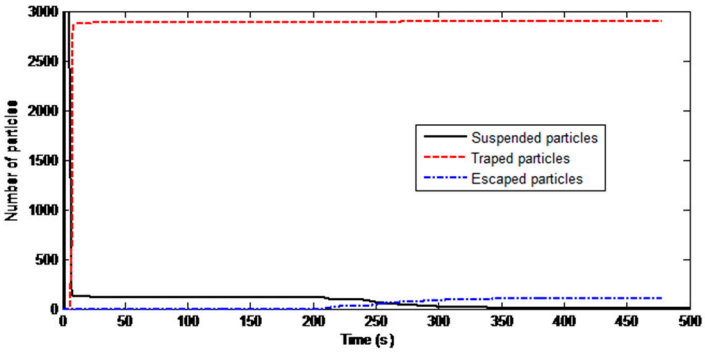
4.3. Chair Displacement

Figure 15 depicts the effect of displacing the chair on the situation of the particles versus time. When the chair is placed in the middle of the room (x = 2 m), more particles collide with it and fewer ones reach the outlet. This may be observed from Figure 15d, where it can be seen that a much larger number of particles will stick to the walls in the case of placing the chair in the middle of the room.

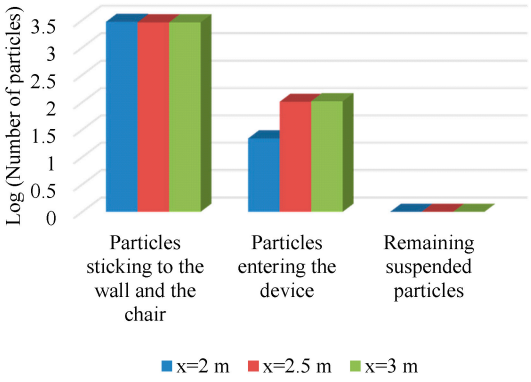


(**a**) x = 2 m (**b**) x = 2.5 m

Figure 15. *Cont.*



(**c**) x = 3 m



(**d**)

Figure 15. Particles situation versus time in the case of presence of a chair in (**a**) x = 2 m, (**b**) x = 2.5 m, and (**c**) x = 3 m; (**d**) The final situation of the particles in the case of displacing the chair.

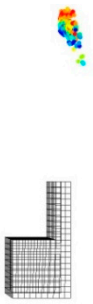
4.4. Air Exit Angle of the Air Cleaner Device

Figure 16a–e illustrates the pattern of particle dispersion at different times within room space. Particles gradually spread in the room according to the flow and reach the device outlet. Figure 16f shows the pathline of the particles selected randomly.

In the following sections, the air exit angle to the device is changed relative to z (left and right from the air cleaner viewpoint) and y (up and down from the air cleaner viewpoint)-axes as shown in Figure 3, and its effect is observed on dispersion and egression of the particles. The number of suspended particles in room space is shown for every moment at different angles to indicate which case is capable of guiding the particles from the room towards the device outlet faster.



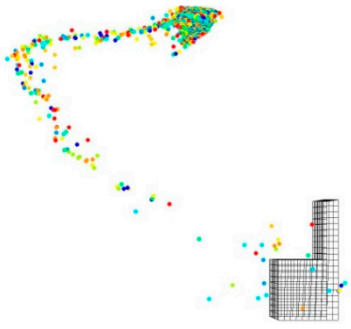
(**a**) t = 1 s



(**b**) t = 5 s

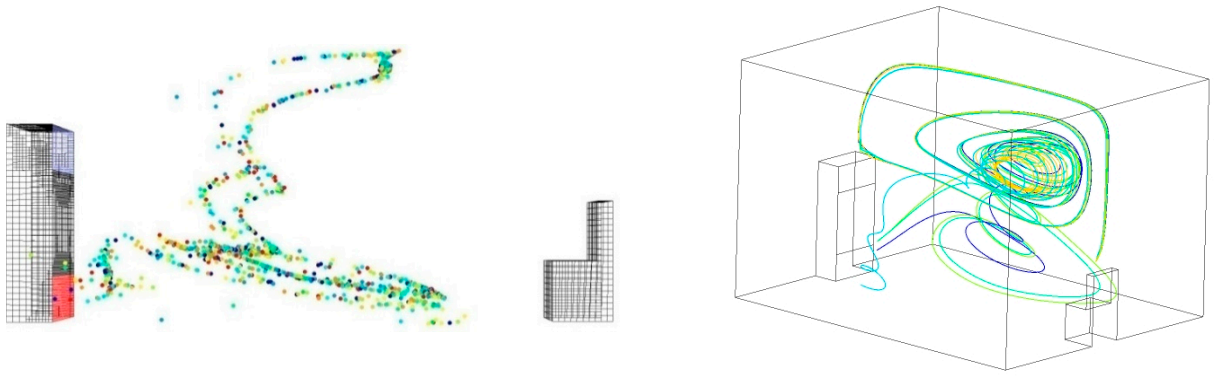


(**c**) t = 50 s



(**d**) t = 150 s

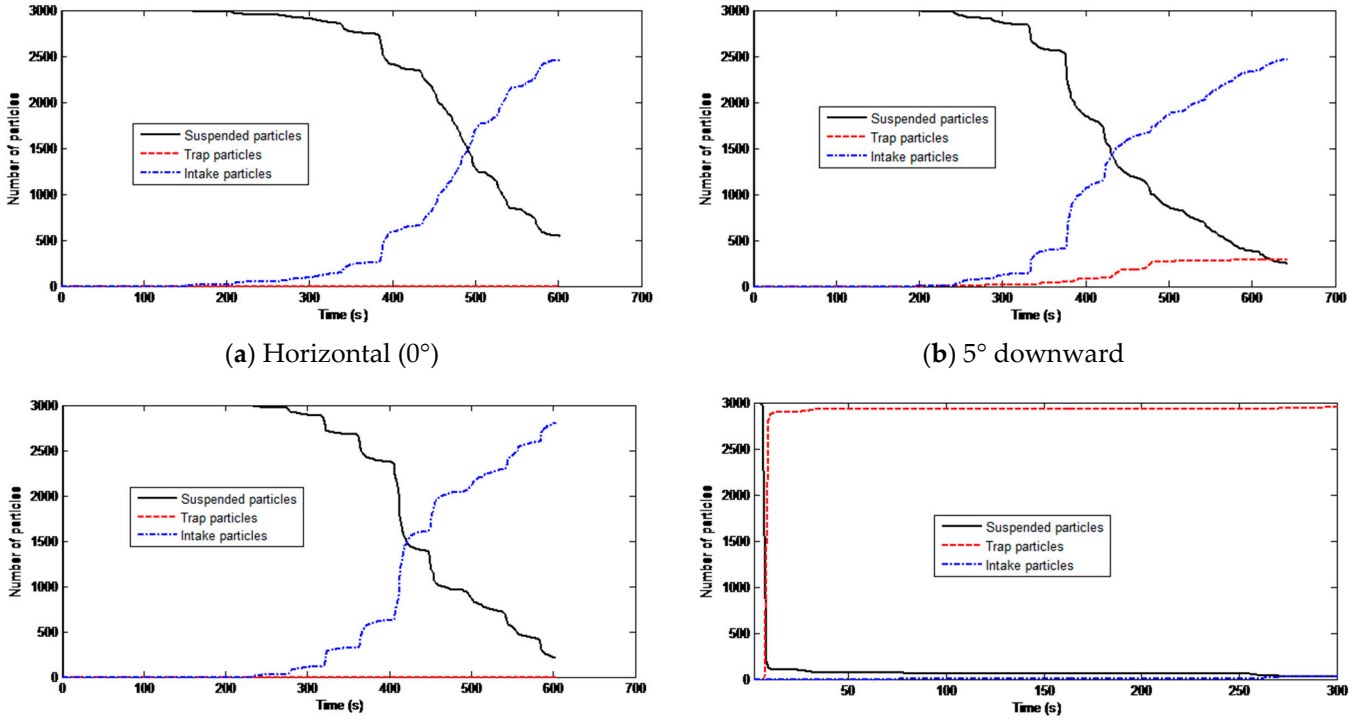
Figure 16. *Cont.*



(**e**) t = 500 s (**f**)

Figure 16. A view of particle positions at different times; (**a**) t = 1 s, (**b**) t = 5 s, (**c**) t = 50 s, (**d**) t = 150 s, and (**e**) t = 500 s, (**f**) The pathlines of a number of particles randomly selected in the room.

The numerical solution is performed here for 0°, 5°, and −5° angles relative to the *z*-axis and the solution was run 600 s for the particles. Figure 17 depicts the number of particles suspended in the air; the particles sticking to the wall, the chair, and the device body; and the particles entering the device over time at different angles. As is clear, in the case of 10° angle downward, approximately all of the particles are absorbed through the device. In the case of 5° angle upward, the airflow causes the particles to stick to the walls and the chair upon injection.



(**a**) Horizontal (0°) (**b**) 5° downward

(**c**) 10° downward (**d**) 5° upward

Figure 17. Particles situation over time for different ejection angles relative to *z*-axis (left and right from the air cleaner viewpoint).

In order to provide a better outlook on the number of particles entering the device, the suspending particles, and the particles sticking to the chair and the walls, a summary of the results is shown in Figure 18. As is shown in Figures 17 and 18, if the ejection angle

is set to a 10° downward, more particles leave the room without sticking to the walls and furniture.

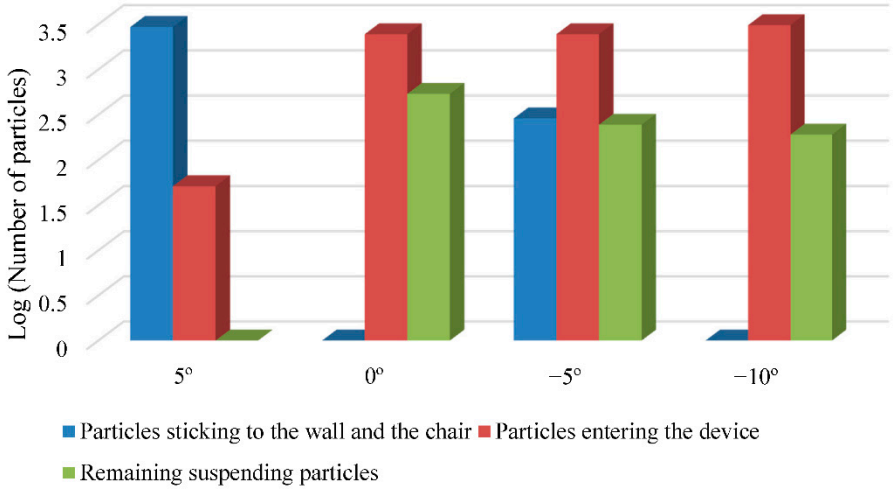
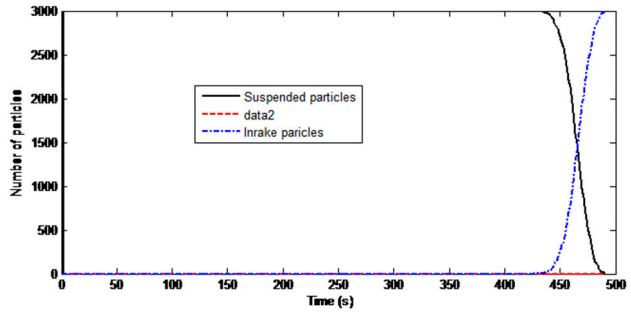
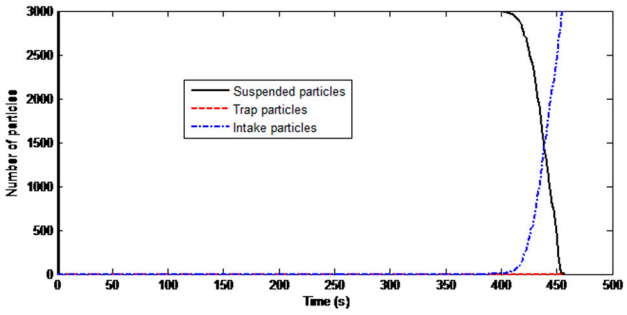


Figure 18. Situation of the particles after 600 s at different ejection angles relative to *z*-axis (left and right from the air cleaner viewpoint).

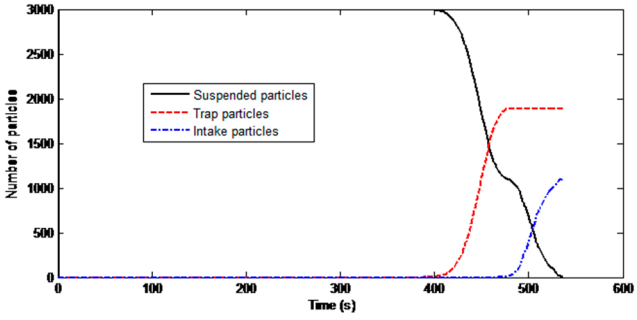
Due to geometric symmetry relative to *y*-axis, only the positive angles are examined here, and the negative angles lead to the same results. As is clear in Figure 19, in the case of 10° and 15° angles relative to *y*-axis, the particles are led towards the outlet faster. However, in the case of 15° angle, a number of particles stick to the wall or the furniture.



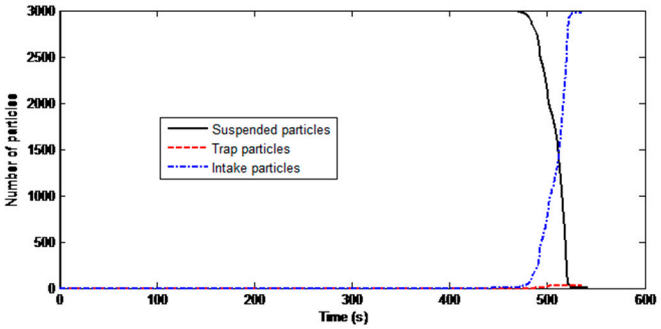
(**a**) 5°



(**b**) 10°



(**c**) 15°



(**d**) 20°

Figure 19. Particles situation over time for different ejection angles relative to *y*-axis (up and down from the air cleaner viewpoint).

In Figure 20, a summary of the results for a few angles under investigation is shown with numerical details. In the case of ejection angle of 10°, the whole particles are directed towards the outlet along with the flow.

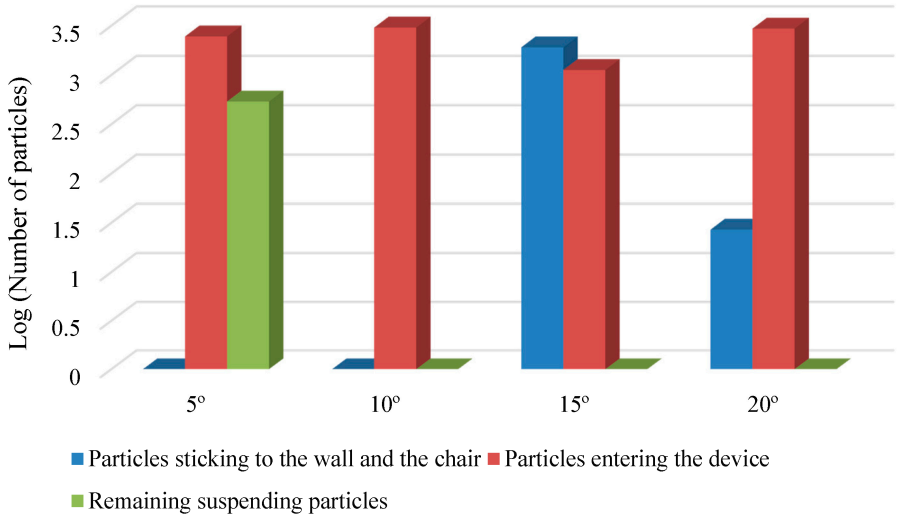


Figure 20. Situation of the particles after 600 s at different vertical ejection angles relative to *y*-axis (up and down from the air cleaner viewpoint).

5. Conclusions

The aim of the current study is to study the effect of the position of the air cleaner device as well as the angle of exit air relative to an air cleaner on dispersion and removal of particles suspending in the air in an isolated room. Computational domain in this study includes an air cleaner device at one side of the room and a chair placed in different places inside the room. It is assumed that a person is standing at the other end of the room and coughing. The effects of placement of the chair and changing the location of air cleaner device on the transport pattern of particles as well as their removal are examined in detail. The impact of the air exit angle from the air cleaner device on dispersion of particles within the room is also studied. For numerical solution, the combination of DPM with the Eulerian fluid model has been employed to predict the transport of particles in the room. Results indicated that when the device is placed in the middle of the larger length of the room, it is capable of removing the particles more efficiently. Additionally, displacing the chair towards the device causes less particles to reach the device. Furthermore, if the ejection angle of air is set to a 10 degree downward, the particles are more easily removed from the space and directed towards the inlet of air cleaner device. Results of the current study may improve the design and utilization of air cleaner devices to achieve higher removal rate of particles in an indoor environment.

Author Contributions: Data curation, F.M.K.; Investigation, F.M.K., M.S. (Mostafa Sefidgar) and S.-A.S.; Methodology, F.M.K., M.S. (Mostafa Sefidgar), S.A. and S.-A.S.; Project administration, M.S. and M.S. (Madjid Soltani); Resources, M.S. (Madjid Soltani) and S.A.; Supervision, M.S. (Mostafa Sefidgar), B.Z.; Validation: F.M.K.; Visualization, F.M.K.; Writing – original draft, F.M.K., S.A. and S.-A.S.; Writing – review & editing, M.S. (Mostafa Sefidgar), M.S. (Madjid Soltani), B.Z.; funding acquisition, M.S. (Madjid Soltani) and B.Z. All authors have read and agreed to the published version of the manuscript.

Funding: This research received no external funding.

Institutional Review Board Statement: Not applicable.

Informed Consent Statement: Not applicable.

Data Availability Statement: Not applicable.

Conflicts of Interest: The authors declare no conflict of interest.

Nomenclature

$\vec{F}$	Volume forces applied to the fluid
$\vec{g}$	Gravitational acceleration vector
I	Unit tensor
k	Turbulence kinetic energy
p	Pressure scalar
S_m	Source term
S_P	Force applied on the fluid by particle in the unit of volume
$\vec{u}$	Continuous phase velocity vector
$\vec{u_p}$	Discrete phase velocity vector
$u'(t)$	Fluctuating velocity
Greek symbols	
ε	Rate of dissipation of turbulence energy
ς	Gaussian random number
μ	Dynamic viscosity
ρ	Density
$\bar{\bar{\tau}}$	Shear stress
Abbreviations	
ACH	Air Changes per Hour
CADR	Clean Air Delivery Rate
CFD	Computational Fluid Dynamics
DRW	Discrete Random Walk
RANS	Reynolds-Averaged Navier-Stokes

References

1. EPA. *Healthy Buildings, Healthy People, a Vision for the 21st Century*; U.S. Environmental Protection Agency: Washington, DC, USA, 2001.
2. Memarzadeh, F.; Xu, W. Role of air changes per hour (ACH) in possible transmission of airborne infections. *Build. Simul.* **2012**, *5*, 15–28. [CrossRef] [PubMed]
3. Faulkner, W.B.; Memarzadeh, F.; Riskowski, G.; Hamilton, K.; Chang, C.-Z.; Chang, J.-R. Particulate concentrations within a reduced-scale room operated at various air exchange rates. *Build. Environ.* **2013**, *65*, 71–80. [CrossRef]
4. Faulkner, W.B.; Memarzadeh, F.; Riskowski, G.; Kalbasi, A.; Ching-Zu Chang, A. Effects of air exchange rate, particle size and injection place on particle concentrations within a reduced-scale room. *Build. Environ.* **2015**, *92*, 246–255. [CrossRef]
5. Kang, S.Y.; Siegel, J.; Novoselac, A. Effective position of portable air cleaning devices in multizone residential buildings. *Indoor Air* **2008**, *644*, 1–8.
6. Novoselac, A.; Siegel, J.A. Impact of placement of portable air cleaning devices in multizone residential environments. *Build. Environ.* **2009**, *44*, 2348–2356. [CrossRef]
7. Kashkooli, F.M.; Soltani, M.; Zargar, B.; Ijaz, M.K.; Taatizadeh, E.; Sattar, S.A. Analysis of an indoor air decontamination device inside an aerobiology chamber: A numerical-experimental study. *Air Qual. Atmos. Health* **2020**, *13*, 281–288. [CrossRef]
8. Noh, K.-C.; Oh, M.-D. Variation of clean air delivery rate and effective air cleaning ratio of room air cleaning devices. *Build. Environ.* **2015**, *84*, 44–49. [CrossRef]
9. Noh, K.-C.; Yook, S.-J. Evaluation of clean air delivery rates and operating cost effectiveness for room air cleaner and ventilation system in a small lecture room. *Energy Build.* **2016**, *119*, 111–118. [CrossRef]
10. Jin, X.; Yang, L.; Du, X.; Yang, Y. Particle transport characteristics in indoor environment with an air cleaner. *Indoor Built Environ.* **2015**, *25*, 987–996. [CrossRef]
11. Chen, L.; Jin, X.; Yang, L.; Du, X.; Yang, Y. Particle transport characteristics in indoor environment with an air cleaner: The effect of nonuniform particle distributions. *Build. Simul.* **2017**, *10*, 123–133. [CrossRef]
12. Nelson, P.R.; Sears, S.B.; Heavner, D.L. Application of methods for evaluating air cleaner performance. *Indoor Built Environ.* **1993**, *2*, 111–117. [CrossRef]
13. Brown, S.K. Assessing the performance of room air cleaners using a room environmental chamber. *Proc. Indoor Air* **1999**, *2*, 647–652.
14. Nazaroff, W.M. Effectiveness of air cleaning technologies. In Proceedings of the Healthy Buildings 2000, the Eighth International Conference on Indoor Air Quality and Climate, Espoo, Finland, 6–10 August 2000; Volume 2, pp. 49–54.
15. Johansson, J.H.P. Impact of room air cleaners on the indoor particle concentration. *Proc. Healthy Build.* **2000**, *2*, 59–60.
16. Ward, M.; Siegel, J.A.; Corsi, R.L. The effectiveness of standalone air cleaners for shelter-in-place. *Indoor Air* **2005**, *15*, 127–134. [CrossRef] [PubMed]

17. Shaughnessy, R.J.; Sextro, R.G. What is an effective portable air cleaning device? A review. *J. Occup. Environ. Hyg.* **2006**, *3*, 169–181. [CrossRef] [PubMed]
18. Sultan, Z.M.; Nilsson, G.J.; Magee, R.J. Removal of ultrafine particles in indoor air: Performance of various portable air cleaner technologies. *Hvac R Res.* **2011**, *17*, 513–525.
19. Association of Home Appliance Manufacturers (AHAM). *In-House Survey of Homes in the United States*; Association of Home Appliance Manufacturers (AHAM): Washington, DC, USA, 2002.
20. Zhao, B.; Zhang, Z.; Li, X. Numerical study of the transport of droplets or particles generated by respiratory system indoors. *Build. Environ.* **2005**, *40*, 1032–1039. [CrossRef] [PubMed]
21. Niu, J.; Tung, T.C.W.; Chui, V.W.Y. Using large environmental chamber technique for gaseous contaminant removal equipment test. *Ashrae Trans.* **1998**, *104*, 1289–1296.
22. Miller, S.L.; Lobascio, C.; Nazaroff, W.W.; Macher, J.M. Effectiveness of in-room air filtration and dilution ventilation for tuberculosis infection control. *J. Air Waste Manag. Assoc.* **1996**, *46*, 869–882. [CrossRef]
23. Sattar, S.A.; Kibbee, R.J.; Zargar, Z.; Wright, K.E.; Rubino, J.R.; Khalid, M.K. Decontamination of indoor air to reduce the risk of airborne infections: Studies on survival and inactivation of airborne pathogens using an aerobiology chamber. *Am. J. Infect. Control* **2016**, *44*, e177–e182. [CrossRef]
24. Akbari, V.; Salmanzadeh, M. Numerical evaluation of the effect of air distribution system and location on performance of a portable air cleaner. *Sci. Technol. Built Environ.* **2019**, *25*, 34–45. [CrossRef]
25. Zargar, B.; Kashkooli, F.M.; Soltani, M.; Wright, K.E.; Ijaz, M.K.; Sattar, S.A. Mathematical modeling and simulation of bacterial distribution in an aerobiology chamber using computational fluid dynamics. *Am. J. Infect. Control* **2016**, *44*, e127–e137. [CrossRef] [PubMed]
26. ANSYS Inc. *ANSYS FLUENT 14.0 Theory Guide*; ANSYS Inc.: Canonsburg, PA, USA, 2012.
27. Mehryan, S.A.M.; Kashkooli, F.M.; Soltani, M. Comprehensive study of the impacts of surrounding structures on the aero-dynamic performance and flow characteristics of an outdoor unit of split-type air conditioner. *Build. Simul.* **2018**, *11*, 325–337. [CrossRef]
28. Soltani, M.; Dehghani-Sanij, A.; Sayadnia, A.; Kashkooli, F.M.; Gharali, K.; Mahbaz, S.B.; Dusseault, M. Investigation of airflow patterns in a new design of wind tower with a wetted surface. *Energies* **2018**, *11*, 1100. [CrossRef]
29. Zhao, B.; Zhang, Y.; Li, X.T.; Yang, X.D.; Huang, D.T. Comparison of indoor aerosol particle concentration and deposition in different ventilated rooms by numerical method. *Build. Environ.* **2004**, *39*, 1–8. [CrossRef]
30. Miller, S.L.; Nazaroff, W.W. Environmental tobacco smoke particles in multizone indoor environments. *Atmos. Environ.* **2001**, *35*, 2053–2067. [CrossRef]
31. Lu, W.; Howarth, A.T.; Adam, N.; Riffat, S.B. Modelling and measurement of airflow and aerosol particle distribution in a ventilated two-zone chamber. *Build. Environ.* **1996**, *31*, 417–423. [CrossRef]